SUPPORTING INFORMATION

Computational design and discovery of "minimally structured" hERG blockers

Andrea Cavalli[*,‡,§], *Rosa Buonfiglio*[‡], *Cristina Ianni* [‡], *Matteo Masetti*[‡], *Luisa Ceccarini*[‡], *Rachel Caves*[†], *Michael W. Y. Chang*[†], *John S. Mitcheson*[†], *Marinella Roberti*[‡] *and Maurizio Recanatini*[‡]

[‡]Department of Pharmaceutical Sciences, University of Bologna, Via Belmeloro 6, I-40126 Bologna, Italy

[§]Department of Drug Discovery and Development, Istituto Italiano di Tecnologia, Via Morego 30, I-16163 Genova, Italy

[†]Department of Biochemistry, University of University of Leicester, University Rd., Leicester LE1 9HN, United Kingdom

RECEIVED DATE (to be automatically inserted after your manuscript is accepted if required according to the journal that you are submitting your paper to)

[*]To whom correspondence should be addressed: Dept. of Pharmaceutical Sciences, Alma Mater Studiorum, Bologna University – via Belmeloro 6, 40126 Bologna, Italy. Phone/Fax: +39 051 2099735/4. Email: andrea.cavalli@unibo.it

Contents (31 pages):

CoMFA model generation

The training set for the CoMFA model contained 75 molecules belonging to different pharmacological classes (antibacterials, antihistamines, antibiotics, antiarrhythmics, and antipsychotics) that are known to cause QT prolongation as consequence of hERG K^+ channel blockade. The test set was composed of 8 compounds here synthesized.

The main source of the activity data was the Fenichel database,[1] otherwise the original literature. Activity data were acquired in the form of IC_{50} values measured by patch clamp on mammalian cells (human embryonic kidney and Chinese hamster ovary). We decided to exclude data obtained in non-mammalian cell lines (*Xenopus laevis* oocytes), since it is recognized that the use of these systems leads to a significant underestimation of a drugs' potency against hERG *in-vivo*.[2,3] When multiple data were reported (HEK and CHO data), the average was calculated and utilized for generating the CoMFA model. Molecular structures of all hERG blockers utilized for the generation of the CoMFA model are reported in Table S1.

Most of the 3D models of the training and test sets molecules were retrieved from the Cambridge Structural Database (CSD).[4] Alternatively, functional groups were added on crystallographic skeletons. Finally, fragments of SYBYL[5] library were used for *de novo* construction of dofetilide, sertindole, and meperidine structures. Geometry optimization calculations were carried out by applying steepest descent and conjugate gradient methods sequentially with a 0.05 kJ mol^{-1} A^{-1} convergence threshold on the gradient. The MMFF94 force field[6,7] was employed for all classical molecular mechanics calculations, since it includes parameters for all the investigated molecules. The conformational search was performed with the Monte Carlo method[8] by means of the MacroModel software.[9] An energy window set equal to 100 kJ mol^{-1} was used as acceptance criterion in order to explore all potentially relevant conformers, and the GB/SA implicit solvation model[10] for water was adopted. The number of Monte Carlo steps was defined according to the flexibility of molecules: 2,000 steps for rigid molecules and 10,000 steps for flexible ones. The main groups of conformers were then identified with the clustering tools implemented in the

MacroModel software. The root-mean-square displacement (rmsd) calculated on the heavy atoms was used as a geometrical similarity metric. The most representative structure of each cluster was selected and optimized at the B3LYP/6-31G* level of theory by means of the Gaussian03 program suite,[11] and RESP charges[12,13] were then derived using the Amber9 package.[14,15]

The CoMFA alignment was based on the crystal structure of astemizole, which perfectly fits the pharmacophoric model of Figure 1. Notably, astemizole is one of the most potent hERG blockers currently known. The identified pharmacophoric points were the basic nitrogen of the piperidine cycle (N), the centers of mass of the two close aromatic rings (C0 and C1) and the center of mass (C2) of the p-methoxyphenyl ring connected to the basic nitrogen by an ethyl chain. Other functional groups, such as halogen atoms in the para position on the phenyl ring (C0) and functions with delocalized π electrons, were also used to improve the fitting. A 3D box was then placed around the aligned molecules (grid spacing of 1 Å and box side of 30 Å) and steric and electrostatic fields (independent variables) were defined at discrete points of the Cartesian space surrounding the molecules by using an sp^3 carbon atom with a formal charge of +1 as a probe. Optimal values of steric and electrostatic field cutoffs were set to 30 and 45 kcal mol^{-1} respectively, to reduce the number of independent variables. A CoMFA standard scaling factor was used and the minimum σ was set to 2.0 kcal mol^{-1}. PLS procedure[16] was chosen to determine the coefficients that best correlate the dependent variable to the independent variables and statistical parameters of cross-validated and non-cross-validated PLS analyses are shown in Table S2. The optimal number of components (latent variables) equal to 3 was defined by evaluating the predictive ability of the model in terms of s_{cross} obtained by a Cross Validated PLS.

In order to challenge the pharmacophore hypothesis, two more conformations of astemizole were used to built two other CoMFA models (see Table S3 for comparison of statistical parameters). The conformational analysis was performed with MacroModel software by setting all parameters as described above. This provides two energetically allowed conformers of astemizole. The eight new compounds were built by means of fragments taken from the SYBYL library, and they were

subjected to the same protocol discussed above. Finally, the charged molecules were aligned using the pharmacophoric hypothesis of Figure 1.

The model possessed satisfactory descriptive ($r^2 = 0.875$ and $s = 0.413$) and predictive ($q^2 = 0.663$ and $s_{cross} = 0.679$) abilities. Furthermore, the hERG blocking potency of an external set, composed by the newly synthesized compounds (see main text), was calculated. The plots of predicted vs. experimental pIC_{50} of 75 training set compounds and compounds **1**-**8** are shown in Figure S2, respectively. Compared to the previous CoMFA model,[17] the wider training set (75 molecules versus 31) enabled a broader chemical space to be covered, leading to a better description of steric and electrostatic contributions. In particular, these two terms seem to be more balanced (Table S2) and both play a significant role, as shown by the contour maps (Figure S3). In addition, the larger training set slightly improved the predictive power of the model, although its overall predictivity was rather low.

In Figure S3, CoMFA contour maps with the pharmacophore frame (Figure S3A) and with the most (Figure S3B) and the least (Figure S3C) potent hERG blockers of the training set are shown. Green and yellow contours represent regions in space where an increasing steric occupancy leads to favorable and unfavorable contributions to the activity, whereas blue and red contours indicate that a favorable effect for activity is achieved with increasing positive and negative charges, respectively. In addition, we also investigated how a neutral hERG blocker (miconazole) fitted with the new CoMFA model. As reported in Figure S4, we can see that miconazole favorably occupied the positive steric region, accounting for its fairly good potency. Conversely, the role of the electrostatic contribution to miconazole hERG blocking activity was much less understandable, probably because our CoMFA model was generated using mainly protonated blockers.

In agreement with experimental data,[18,19] we predicted astemizole as the most potent hERG blocker, as it fully satisfied the C0, C1, C2, and N pharmacophoric requirements for high affinity binding to the channel. Conversely, the weakest blocker, methylecgonidine, did not place any moieties into the favorable steric regions. In fact, this molecule extended within the blue

electrostatic contour with the ester group, which carries a partial negative charge detrimental, in that region, for hERG activity.

Table S1. Training set molecules and activity data extracted from Fenichel's database.

TRAINING SET		
Compound name	**Structure**	**pIC_{50}**
2-hydroxymethyl olanzapine (**18**)	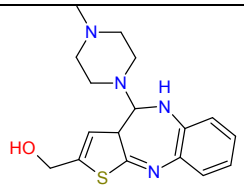	4.9[20]
9-hydroxy risperidone (**19**)	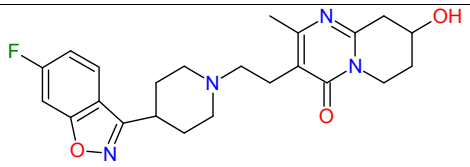	5.9[20]
ajmaline (**20**)	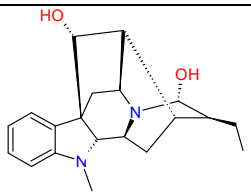	6.0[21]
alfuzosin (**21**)	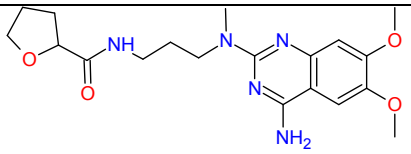	4.1
alosetron (**22**)	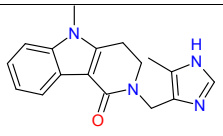	5.5[20]

amitriptyline (**23**)	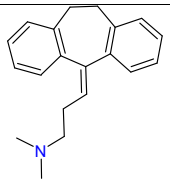	5.0
amsacrine (**24**)	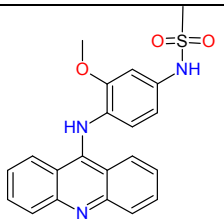	6.7[22]
aprinidine (**25**)	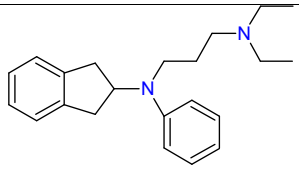	6.6
astemizole (**26**)	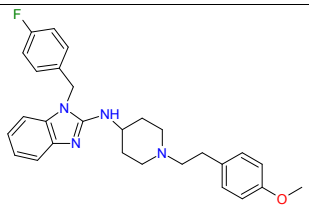	9.0[18]
azimilide (**27**)	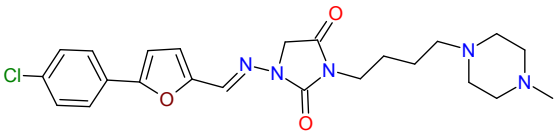	6.2[23]
bepridil (**28**)	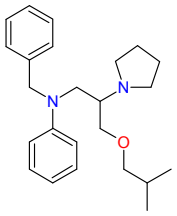	6.3
buprenorphine (**29**)	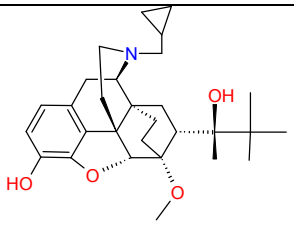	5.1
chlorpromazine (**30**)	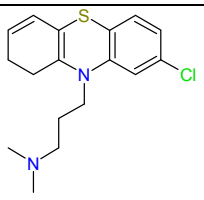	5.8

cisapride (**31**)	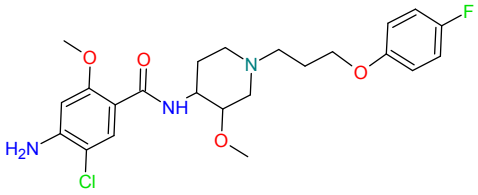	7.7
citalopram (**32**)	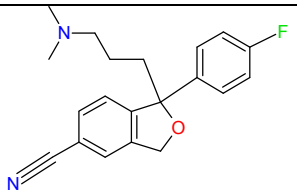	5.4[24]
clobutinol (**33**)	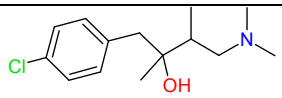	5.5
clomifene (**34**)	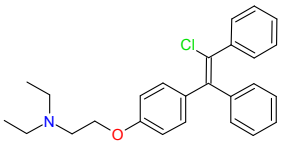	6.7[25]
clozapine (**35**)	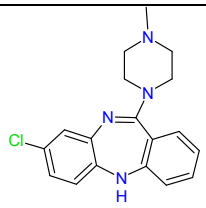	6.7
clozapine N-oxide (**36**)	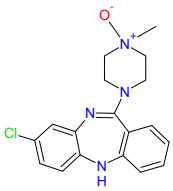	3.9[20]
cocaethylene (**37**)	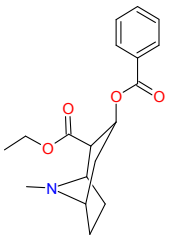	5.9[26]
cocaine (**38**)	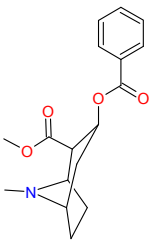	5.1

desipramine (**39**)	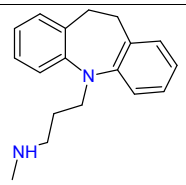	5.9[20]
desloratadine (**40**)	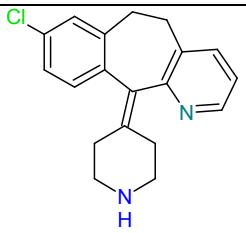	5.2[27]
diltiazem (**41**)	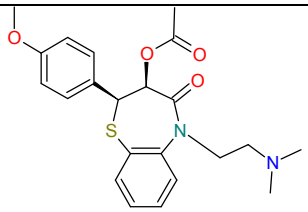	4.8
dofetilide (**42**)	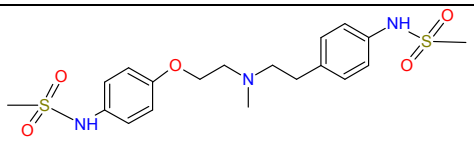	7.9
dolasetron (**43**)	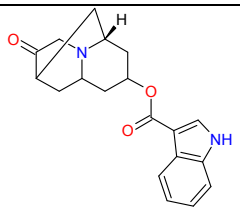	5.2[28]
domperidone (**44**)	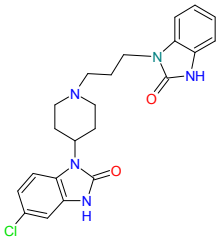	6.8[29]
doxazosin (**45**)	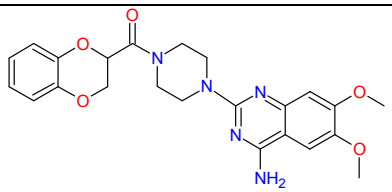	5.6

droperidol (**46**)	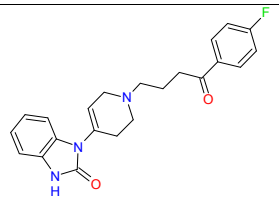	7.5[30]
E-4031 (**47**)	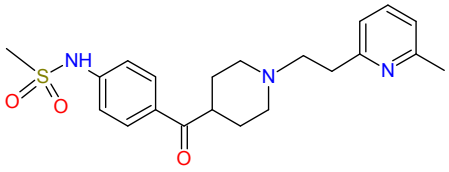	8.1
fentanyl (**48**)	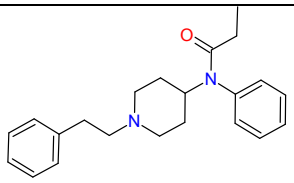	5.7
fexofenadine (**49**)	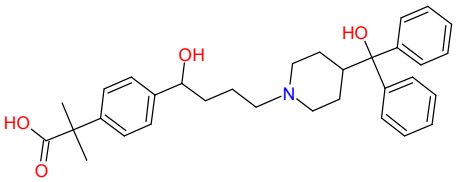	4.7
gatifloxacin (**50**)	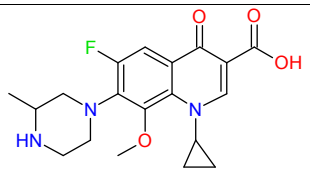	3.9
glibenclamide (**51**)	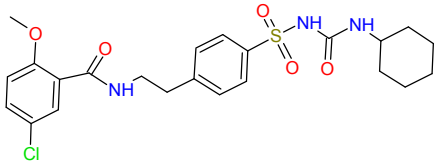	4.1
granisetron (**52**)	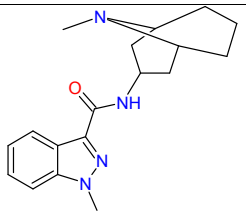	5.4[28]
grepafloxacin (**53**)	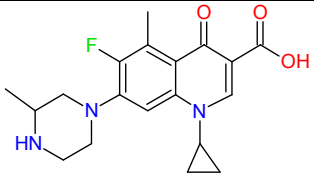	4.4

halofantrine (**54**)	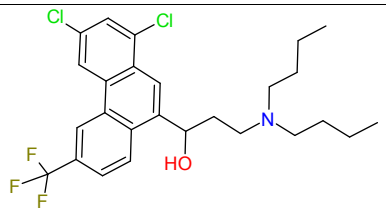	7.3[31-33]
haloperidol (**55**)	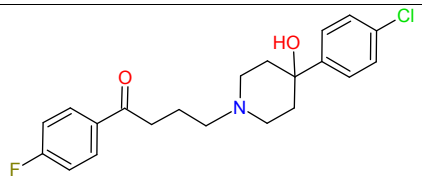	7.6
imipramine (**56**)	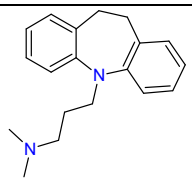	5.5
ketoconazole (**57**)	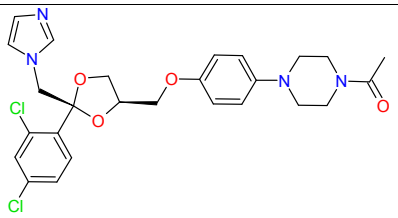	5.8[34]
LAAM (**58**)	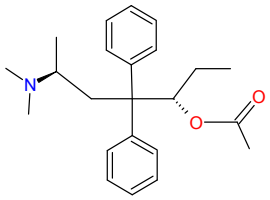	5.7
levobupivacaine (**59**)	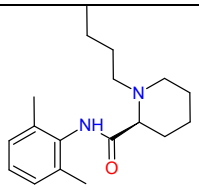	5.0[35]
lidoflazine (**60**)	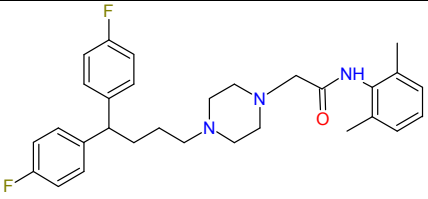	7.8[36]

loratadine (**61**)	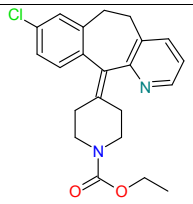	6.1[37,38]
mefloquine (**62**)	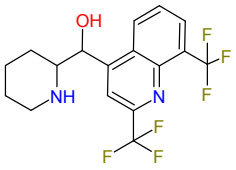	5.4[33,39]
meperidine (**63**)	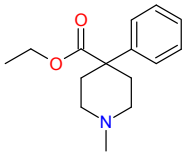	4.1
mesoridazine (**64**)	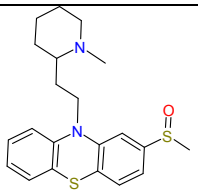	6.3[40]
methadone (**65**)	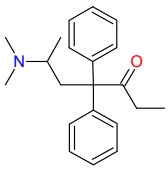	5.0
methylecgonidine (**66**)	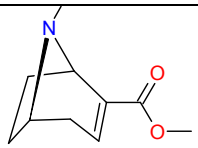	3.8[26]
metoclopramide (**67**)	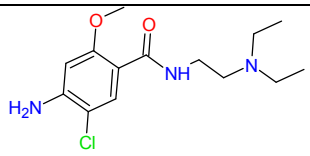	5.3[41]
miconazole (**68**)	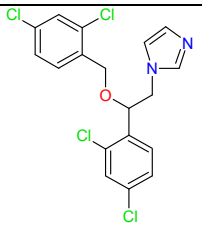	5.7[42]

mizolastine (**69**)	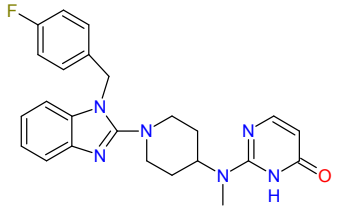	6.5[43]
moxifloxacin (**70**)	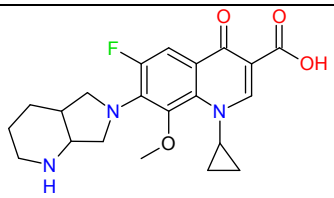	4.8
norastemizole (**71**)	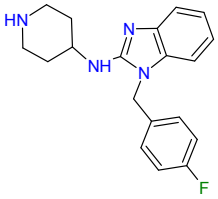	7.6[18]
N-desbutyl halofantrine (**72**)	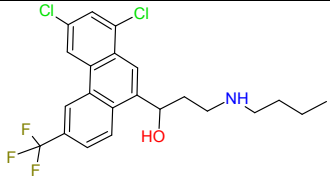	7.1[32]
N-desmethyl clozapine (**73**)	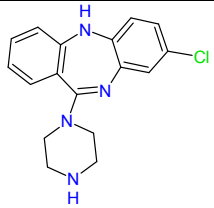	5.4[20]
N-desmethyl olanzapine (**74**)	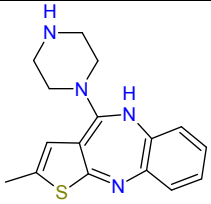	4.9[20]
olanzapine (**75**)	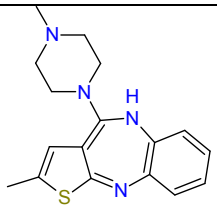	6.7

perhexiline (**76**)	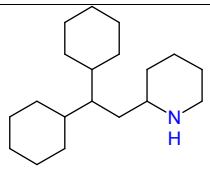	5.1
perphenazine (**77**)	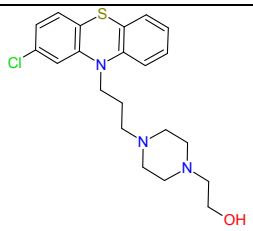	6.0[44]
pilsicainide (**78**)	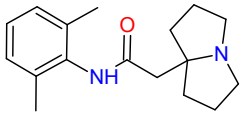	4.7[45]
pimozide (**79**)	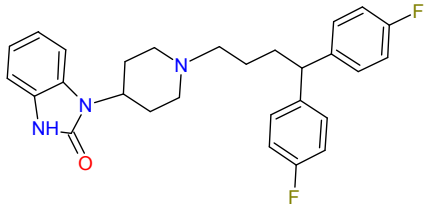	7.5
prazosin (**80**)	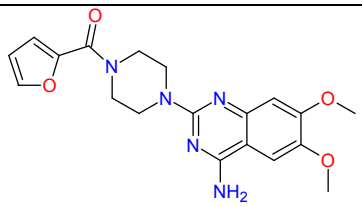	5.5
quetiapine (**81**)	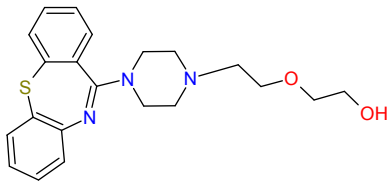	5.2[46]
risperidone (**82**)	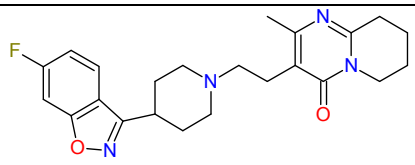	6.8[46]
ropivacaine (**83**)	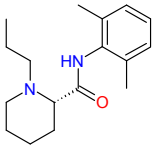	4.6[47]

sertindole (**84**)	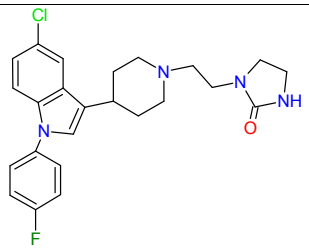	7.9
sparfloxacin (**85**)	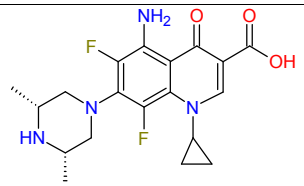	4.8
terazosin (**86**)	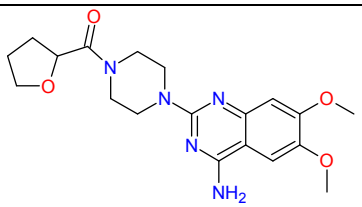	4.7
terfenadine (**87**)	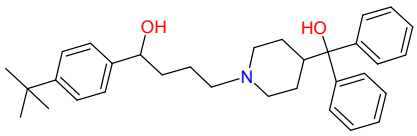	7.0
thioridazine (**88**)	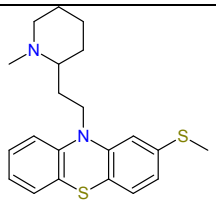	6.7
trazodone (**89**)	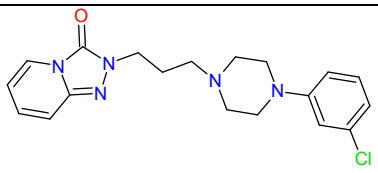	5.9[48,49]
trifluoperazine (**90**)	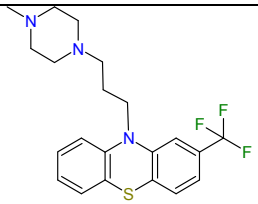	5.9[44]
verapamil (**91**)	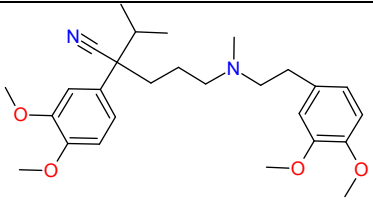	6.8

ziprasidone (**92**)	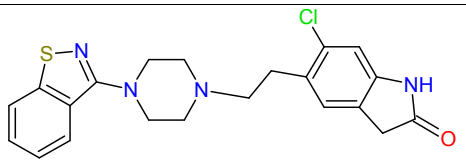	6.8

Table S2. Summary of the CoMFA statistical parameters.

q^2	0.663
s_{cross}	0.679
F	166.021
r^2	0.875
S	0.413
optimal number of components	3
steric field contribution	0.569
electrostatic field contribution	0.431

Table S3. Statistical parameters of the CoMFA model based on the crystal structure of astemizole (second column) and two more conformers (third and fourth columns).

	CoMFA model based on crystal structure of astemizole	CoMFA model 2	CoMFA model 3
q^2	0.663	0.243	0.327
s_{cross}	0.679	1.135	1.009
r^2	0.875	0.702	0.624
S	0.413	0.647	0.726
optimal number of components	3	3	3

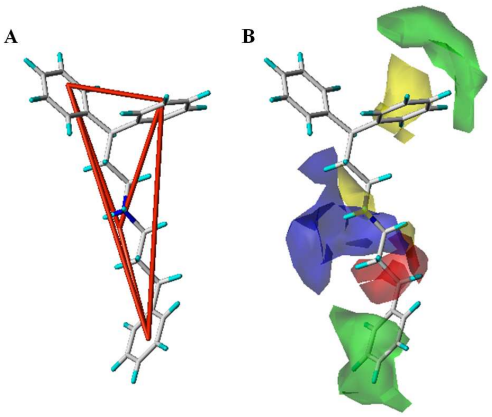

Figure S1. A) Superimposition of **2** and the pharmacophore model of Figure 1. B) Steric and electrostatic CoMFA STDEV*COEFF contour maps with compound **2**. **2** can fit with the pharmacophoric functions thought to be responsible for hERG activity.

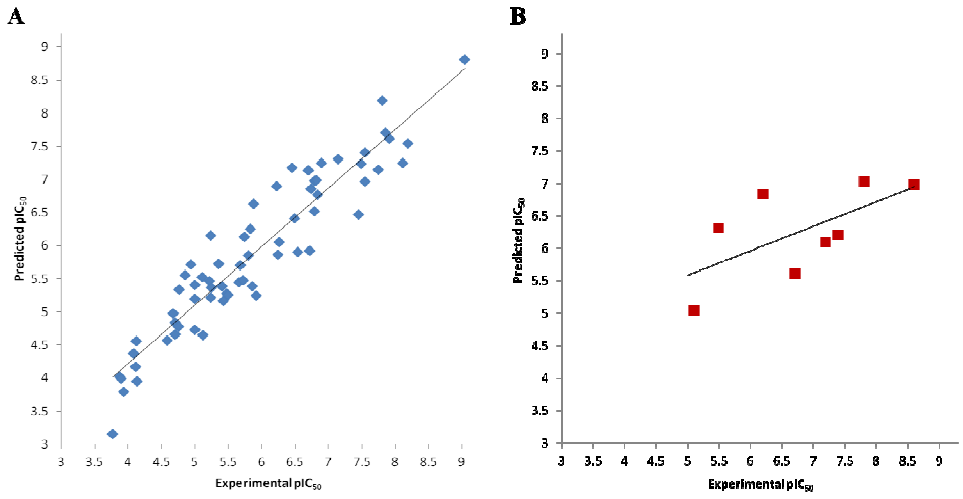

Figure S2. A) Plot of predicted vs. experimental pIC_{50} of 75 training set compounds. B) The same plot for compounds **1-8**. Predicted activities were calculated from the non-cross-validated CoMFA model.

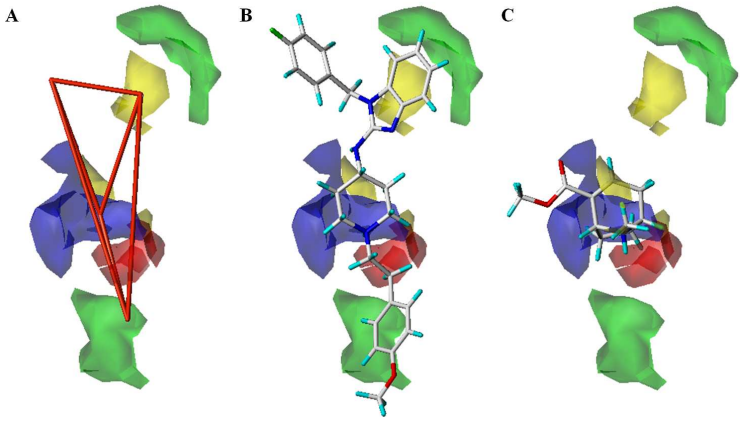

Figure S3. A) Steric and electrostatic CoMFA STDEV*COEFF contour maps plotted together with the pharmacophore model reported in Figure 1. B) and C) The same contour maps with astemizole and methylecgonidine. In all panels, positive (0.0052) and negative (-0.0031) CoMFA steric contours are shown in green and yellow, respectively. Positive (0.0035) and negative (-0.0052) CoMFA electrostatic contours are shown in blue and red, respectively.

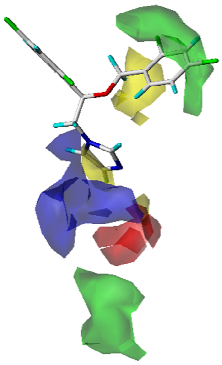

Figure S4. Steric and electrostatic CoMFA STDEV*COEFF contour maps plotted together with miconazole as example of uncharged hERG blocker.

Chemistry

General chemical methods

Reaction progress was monitored by TLC on precoated silica gel plates (Kieselgel 60 F_{254}, Merck) and visualized by UV254 light. Flash column chromatography was performed on silica gel (particle size 40-63 Mm, Merck). All the solvents were freshly distilled. Unless otherwise stated, all reagents were obtained from Sigma-Aldrich and used without further purification. Compounds were

named relying on the naming algorithm developed by CambridgeSoft Corporation and used in Chem-BioDraw Ultra 11.0. ^{1}H-NMR and ^{13}C-NMR spectra were recorded at 200-300 and 50-75 MHz, respectively. Chemical shifts (ppm) are reported relative to TMS as internal standard. Coupling constants (J), when given, are reported in Hertz (Hz). IR-FT spectra were performed in Nujol and obtained on a Nicolet Avatar 320 E.S.P. instrument; ν value max is expressed in cm-1. Mass spectra were recorded on a V.G. 7070 E spectrometer or on a Waters ZQ 4000 apparatus operating in electrospray (ES) mode. Purity of compounds was determined by elemental analyses; purity for all the tested compounds was ≥ 95%. The parallel synthetic reactions were carried out into the Carousel station by Radleys Discovery Technologies composed of 12 reactors.

General parallel procedure for the synthesis of (N-phenylalkyl) diphenylalkylamine and (N1,N1-diphenyl,N2-phenylalkyl) alkylene diamines derivatives 1-6 (Scheme 1 in the main text)

In distinct reactors, the appropriate amines **9**, **10**, **11** (1.0 equiv) were dissolved in methanol dry (3.5 mL), then 2-phenylacetaldehyde and 3-phenylpropanal **12**, **13** (1.3 equiv) were added to the corresponding reactors, followed by the addition to each reactors of $NaBH_3CN$ (1.5 equiv). The resulting mixtures were left at room temperature and allowed to stir for seven days, and then each one was treated as follows: each mixture was washed with MeOH and evaporated, the resulting residue was taken up in CH_2Cl_2, the solid material was filtered off and the organic solution was concentrated *in-vacuo*. The final compound was purified by flash column chromatography and salified by adding hydrochloric acid 1 M (1 equiv).

Characterization of compounds 1-6

N-phenethyl-3,3-diphenylpropan-1-amine (1). 3,3-diphenylpropan-1-amine 9 (0.3 g, 1.42 mmol), 2-phenylacetaldehyde 12, $NaBH_3CN$ (0.13 g) were allowed to react according to the described general procedure and the crude product was purified on silica eluting with 5: 5

petroleum ether: EtOAc. 1: 0.157 g (yield 35 %); white fine powder; ^{1}H-NMR ($CDCl_3$, 200 MHz) δ 1.24 (s br, 1H), 2.23-2.35 (m, 2H), 2.52-2.71 (m, 2H), 2.84-2.87 (m, 4H), 3.97 (t, *J* = 7.8 Hz, 1H), 7.09-7.38 (m, 15H). ^{13}C-NMR ($CDCl_3$ 75 MHz,) δ 35.1, 36.6, 37.0, 47.9, 48.9, 126.4, 126.6, 127.62, 127.67, 128.5, 128.7, 143.3, 143.9, 161.0, 164.6. MS (ES): m/z 316 ($M+H^+$).

3,3-diphenyl-*N*-(3-phenylpropyl)propan-1-amine (2). 3,3-diphenylpropan-1-amine **9** (0.2 g, 0.95 mmol), 3-phenylpropanal **13**, $NaBH_3CN$ (0.09 g) were allowed to react according to the described general procedure and the crude product was purified on silica eluting with 9: 1 EtOAc: MeOH. **2**: 0.136 g (yield 43 %); white fine powder; ^{1}H-NMR (DMSO-d_6, 200 MHz) δ 1.87-1.91 (m, 2H), 2.38-2.83 (m, 8H), 4.09 (t, *J* = 7.6 Hz, 1H), 7.18-7.31 (m, 15H), 9.06 (s br, 1H). ^{13}C-NMR ($CDCl_3$, 75 MHz) δ 29.9, 33.1, 34.2, 47.7, 48.5, 48.9, 125.9, 126.3, 127.6, 128.2, 128.3, 128.5, 141.1, 144.0.

***N*^{1}-phenethyl-*N*^{2},*N*^{2}-diphenylethane-1,2-diamine (3).** N^1,N^1-diphenylethane-1,2-diamine **10** (0.25 g 1.2 mmol), 2-phenylacetaldehyde **12**, $NaBH_3CN$ (0.11 g) were allowed to react according to the described general procedure and the crude product was purified on silica eluting with 7: 3 petroleum ether: EtOAc. **3**: 0.145 g (yield 38 %); whitish granular powder; ^{1}H-NMR ($CDCl_3$, 200 MHz) δ 2.87-2.96 (m, 6H), 3.91-3.95 (m, 2H), 6.96-6.99 (m, 5H), 7.16-7.26 (m, 10H), 9.12 (s, br 1H). ^{13}C-NMR ($CDCl_3$, 75 MHz) δ 36.0, 46.9, 51.0, 51.7, 121.0, 121.4, 126.1, 128.4, 128.6, 129.2, 129.5, 139.5, 147.8.

***N*^{1},*N*^{1}-diphenyl-*N*^{2}-(3-phenylpropyl)ethane-1,2-diamine (4).** N^1,N^1-diphenylethane-1,2-diamine **10** (0.3 g, 1.4 mmol), 3-phenylpropanal **13**, $NaBH_3CN$ (0.13 g) were allowed to react according to the described general procedure and the crude product was purified on silica eluting with 7: 3 petroleum ether: EtOAc. **4:** 0.198 g (yield 43 %); whitish granular powder; ^{1}H-NMR (DMSO-d_6, 200 MHz) δ 1.87-2.08 (m, 2H), 2.60-2.67 (m, 2H), 2.92-3.08 (m, 4H), 4.03 (m, 2H), 6.94-7.05 (m, 5H), 7.18-7.33 (m, 10H), 9.09 (s, br 1H). ^{13}C-NMR ($CDCl_3$, 75 MHz) δ 31.4, 33.4, 47.1, 49.2, 51.8, 121.0, 121.4, 125.7, 128.3, 129.2, 141.8, 147.9.

***N*^{1},*N*^{1}–bis(4-fluorophenyl)-*N*^{2}–phenetylethane-1,2-diamine (5).** N^1,N^1-bis(4-fluorophenyl) ethane-1,2-diamine **11** (0.4 g, 1.6 mmol), 2-phenylacetaldehyde **12**, $NaBH_3CN$ (0.15 g) were allowed to react according to the described general procedure and the crude product was purified on silica eluting with 6: 4 petroleum ether: EtOAc. **5:** 0.116 g (yield 30 %); white fine powder; ^{1}H-NMR (DMSO-d_6, 200 MHz) δ 2.95-3.13 (m, 6H), 3.95-3.99 (m, 2H), 7.00-7.32 (m, 13H), 9.25 (s, br 1H). ^{13}C-NMR (DMSO-d_6, 75 MHz) δ 31.5, 43.5, 47.8, 48.1, 115.8, 116.2, 122.4, 122.5, 126.7, 128.6, 137.1, 143.64, 143.69, 155.1, 159.9.

***N*^{1},*N*^{1}–bis(4-fluorophenyl)-*N*^{2}–(3-phenylpropyl)ethane-1,2-diamine (6).** N^1,N^1-bis(4-fluorophenyl) ethane-1,2-diamine **11** (0.45 g, 1.18 mmol), 3-phenylacetaldehyde **13**, $NaBH_3CN$ (0.17 g) were allowed to react according to the described general procedure and the crude product was purified on silica eluting with 6: 4 petroleum ether: EtOAc. **6:** 0.113 g (yield 26 %); white fine powder; ^{1}H-NMR ($CDCl_3$, 200 MHz) δ 1.79-1.90 (m, 2H), 2.62-2.69 (m, 4H), 2.82-2.88 (m, 2H), 3.79 (t, J = 6.6 Hz), 6.94-7.02 (m, 8H), 7.15-7.33 (m, 5H), 9.00 (s, br 1H). ^{13}C-NMR (DMSO-d_6, 75 Hz) δ 27.5, 32.2, 43.7, 46.8, 48.4, 116.1, 116.6, 122.7, 122.8, 126.3, 128.5, 128.7, 140.9, 143.93, 143.97.

General procedure for the synthesis of (N1,N1-diphenyl,N2-phenylalkylamide) alkylene amine derivatives 7-8 (Scheme 2 in the main text)

In distinct reactors the appropriate amines **10**, **11** (1.0 equiv) were dissolved in methanol dry (7 mL). The solutions, under nitrogen atmosphere, were cooled to 0° C then diisopropylethylamine (2.0 equiv) was added, followed by the portionwise addition of 2-phenylacetyl chloride **14** and 3-phenylpropanoyl chloride **15** (1.5 equiv) respectively. The resulting mixtures were allowed to stir for 4h at room temperature, then each one was treated as follows: each mixture was concentrated to near dryness, and dissolved in CH_2Cl_2. The organic phase were washed with brine, dried over sodium sulfate and evaporated *in vacuo.* The final compounds were purified by flash column chromatography.

Characterization of compounds 7-8

***N*-(2-(diphenylamino)ethyl)-2-phenylacetamide (7).** N^1,N^1-diphenylethane-1,2-diamine **10** (0.2 g, 0.94 mmol), diisopropylethylamine (0.24 g) and 2-phenylacetyl chloride **14**, were allowed to react according to the described general procedure and the crude product was purified on silica eluting with 7.8: 2.2 petroleum ether: EtOAc. **7:** 0.140 g (yield 53 %); light grey powder; ^{1}H-NMR ($CDCl_3$, 300 MHz) δ 3.41-3.45 (m, 2H), 3.50 (s, 2H), 3.80-3.83 (m, 2H), 5.55 (s br, 1H), 6.87-6.96 (m, 6H), 7.12-7.14 (m, 2H), 7.19-7.31 (m, 7H). ^{13}C-NMR ($CDCl_3$ 75 MHz,) δ 37.84, 43.95, 50.86 , 121.12, 121.84, 127.53, 129.19, 129.54, 129.69, 134.77, 147.83, 171.40.

***N*-(2-(bis(4-fluorophenyl)amino)ethyl)-3-phenylpropanamide (8).** N^1,N^1-bis(4-fluorophenyl) ethane-1,2-diamine **11** (0.25 g, 1.01 mmol), diisopropylethylamine (0.26 g) and 3-phenylpropanoyl chloride **15**, were allowed to react according to the described general procedure and the crude product was purified on silica eluting with 7.6: 2.4 petroleum ether: EtOAc. **8**: 0.220 g (yield 57 %); white fine powder; ^{1}H-NMR ($CDCl_3$, 300 MHz) δ 2.42 (t, *J*= 7.6 Hz, 2H), 2.92 (t, *J*= 7.6, 2H), 3.37-3.42 (m, 2H), 3.67-3.71 (m, 2H), 5.49 (s br, 1H), 6.85-6.98 (m, 8H), 7.15-7.20 (m, 3H), 7.23-7.28 (m, 2H). ^{13}C-NMR ($CDCl_3$ 75 MHz) δ 31.69, 37.63, 38.49, 51.72, 116.15, 116.37, 122.40, 122.48, 126.46, 128.45, 128.71, 140.81, 144.36, 157.07, 159.46, 172.58.

Scheme S1.

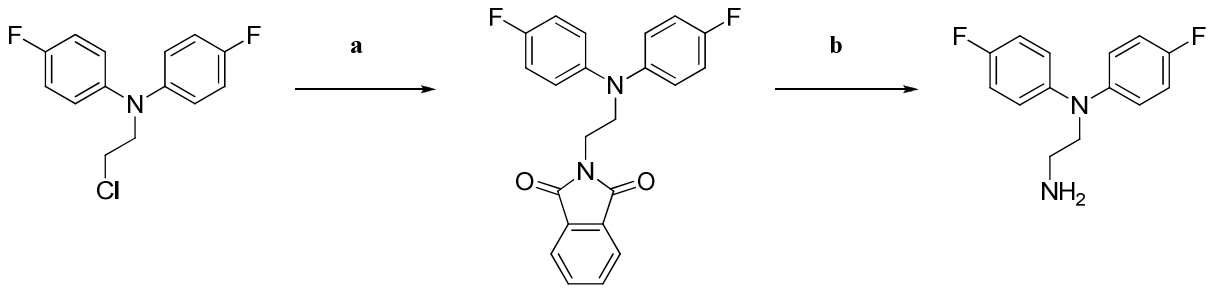

16 **17** **11**

Reagents and conditions: (a) Potassium phthalimide, DMF dry, reflux 3 h; (b) Hydrazine Hydrate, EtOH, reflux 1 h.

Procedures to obtain compounds 17 and 11 and their characterization

2-(2-(bis(4-fluorophenyl)amino)ethyl)isoindoline-1,3-dione (17). In a three-neck flask under N_2 atmosphere, N-(2-chloroethyl)-4-fluoro-N-(4-fluorophenyl)aniline **16** (1.5 g, 5.60 mmol), was dissolved in DMF dry (10 mL). To this solution potassium phthalimide (1.56 g, 8.40 mmol) was added and the resulting mixture was brought to reflux and allowed to stir for 3 h. After this time the mixture reaction was poured in crushed ice and extracted with Et_2O. The combined organic layers were dried with Na_2SO_4 and evaporated. The crude yellow solid was purified by flash cromatography eluting with 9: 1 petroleum ether: EtOAc. **17:** 1.28g (yield 60.4 %); ^{1}H-NMR ($CDCl_3$, 200 MHz) δ 3.98 (s, 4H), 6.94-6.98 (m, 8H), 7.71-7.85 (m, 4H).

***N*^{1},*N*^{1}-bis(4-fluorophenyl)ethane-1,2-diamine (11).** A solution of 2-(2-bis(4-fluorophenyl)amino)ethyl)isoindoline-1,3-dione **17** (1.30 g, 3.44 mmol) and hydrazine hydrate (0.80 mL, 25.77 mmol) in EtOH and under N_2 atmosphere (30 mL), was heated to reflux for 1 h. After this time, the resulting white spongy residue was filtered off, while the solution was concentrated. After solvent evaporation a small residue was formed, filtered off and the solution was concentrated. The crude compound was purified with flash chromatography eluting with 9.85: 0.15 CH_2Cl_2: MeOH on silica saturated for the 50 % with NH_3. **11:** 0.79 g (yield 92.6 %); ^{1}H-NMR ($CDCl_3$, 200 MHz) δ 1.67 (s, br 2H), 2.94 (t, *J* = 6.6 Hz, 2H), 3.73 (t, *J* = 6.6 Hz, 2H), 6.94-6.97 (m, 8H).

Patch clamp experiments

The biological activity of compounds **1**-**8** was determined by measuring inhibition of hERG currents using the whole-cell configuration of the patch-clamp technique as described previously,[50] in stably transfected HEK cells (kindly provided by Prof Craig January (University of Wisconsin). Cells were superfused with room temperature extracellular Tyrode containing (in mM), NaCl 140, $MgCl_2$ 1, KCl 4, Glucose 10, HEPES 5, $CaCl_2$ 2, pH 7.4. Stock solutions of the compounds (in DMSO) were diluted in Tyrode to the desired concentrations. Total DMSO was < 0.1%.

Borosilicate glass pipettes (Harvard Apparatus) with final resistances of 2 to 4 MΩ were filled with an intracellular solution containing (in mM), KCl 130, MgATP 5, HEPES 10, pH 7.2. Cells were voltage clamped at a holding potential of -80 mV and hERG currents activated with repetitive application of 5-s pulses to 0 mV followed by a repolarising pulse to -50 mV to elicit tail currents. Peak tail current amplitudes following steady-state inhibition were measured, leak current subtracted, normalised to current in control Tyrode and the resulting concentration-response relationships from individual cells fitted with a Hill function to obtain IC_{50} and slope values. Mean pIC_{50} results for each compound are from 5-9 cells.

References

1. Fenichel, R.R.http://www.fenichel.net/pages/Professional/subpages/QT/Tables/pbydrug.htm

2. Cavero, I.; Mestre, M.; Guillon, J. M.; Crumb, W. Drugs that prolong QT interval as an unwanted effect: assessing their likelihood of inducing hazardous cardiac dysrhythmias. *Expert. Opin. Pharmacother.* **2000**, *1*, 947-973.

3. Netzer, R.; Ebneth, A.; Bischoff, U.; Pongs, O. Screening lead compounds for QT interval prolongation. *Drug. Discov. Today.* **2001**, *6*, 78-84.

4. Fletcher, D. A.; McMeeking, R. F.; Parkin, D. The United Kingdom Chemical Database Service. *J. Chem. Inform. Comput. Sci.* **1996**, *36*, 746-749.

5. SYBYL 7.3; Tripos International: St. Louis, MO. **2006**.

6. Halgren, T. A. Merck molecular force field. I. Basis, form, scope, parameterization, and performance of MMFF94. *J. Comput. Chem.* **1996**, *17*, 490-519.

7. Halgren, T. A. Merck molecular force field. II. MMFF94 van der Waals and electrostatic parameters for intermolecular interactions. *J. Comput. Chem.* **1996**, *17*, 520-552.

8. Chang, G.; Guida, W. C.; Still, W. C. An internal-coordinate Monte Carlo method for searching conformational space. *J. Am. Chem. Soc.* **1989**, *111*, 4379-4386.

9. Mohamadi, F.; Richards, N. G. J.; Guida, W. C.; Liskamp, R.; Lipton, M.; Caufield, C.; Chang, G.; Hendrickson, T.; Still, W. C. Macromodel—an integrated software system for modeling organic and bioorganic molecules using molecular mechanics. *J. Comput. Chem.* **1990**, *11*, 440-467.

10. Qiu, D.; Shenkin, P. S.; Hollinger, F. P.; Still, W. C. The GB/SA Continuum Model for Solvation. A Fast Analytical Method for the Calculation of Approximate Born Radii. *J. Phys. Chem. A.* **1997**, *101*, 3005-3014.

11. Frisch, M. J. T., G. W.; Schlegel, H. B.; Scuseria, G. E.; Robb, M. A.; Cheeseman, J. R.; Montgomery, Jr., J. A.; Vreven, T.; Kudin, K. N.; Burant, J. C.; Millam, J. M.; Iyengar, S. S.; Tomasi, J.; Barone, V.; Mennucci, B.; Cossi, M.; Scalmani, G.; Rega, N.; Petersson, G. A.; Nakatsuji, H.; Hada, M.; Ehara, M.; Toyota, K.; Fukuda, R.; Hasegawa, J.; Ishida, M.; Nakajima, T.; Honda, Y.; Kitao, O.; Nakai, H.; Klene, M.; Li, X.; Knox, J. E.; Hratchian, H. P.; Cross, J. B.; Bakken, V.; Adamo, C.; Jaramillo, J.; Gomperts, R.; Stratmann, R. E.; Yazyev, O.; Austin, A. J.; Cammi, R.; Pomelli, C.; Ochterski, J. W.; Ayala, P. Y.; Morokuma, K.; Voth, G. A.; Salvador, P.; Dannenberg, J. J.; Zakrzewski, V. G.; Dapprich, S.; Daniels, A. D.; Strain, M. C.; Farkas, O.; Malick, D. K.; Rabuck, A. D.; Raghavachari, K.; Foresman, J. B.; Ortiz, J. V.; Cui, Q.; Baboul, A. G.; Clifford, S.; Cioslowski, J.; Stefanov, B. B.; Liu, G.; Liashenko, A.; Piskorz, P.; Komaromi, I.; Martin, R. L.; Fox, D. J.; Keith, T.; Al-Laham, M. A.; Peng, C. Y.; Nanayakkara, A.; Challacombe, M.; Gill, P. M. W.; Johnson, B.; Chen, W.; Wong, M. W.; Gonzalez, C.; and Pople, J. A. Gaussian 03, Revision C.02, Gaussian, Inc., Wallingford CT. **2004**.

12. Cornell, W. D.; Cieplak, P.; Bayly, C. I.; Kollmann, P. A. Application of RESP charges to calculate conformational energies, hydrogen bond energies, and free energies of solvation. *J. Am. Chem. Soc.* **1993**, *115*, 9620-9631.

13. Bayly, C. I.; Cieplak, P.; Cornell, W.; Kollman, P. A. A well-behaved electrostatic potential based method using charge restraints for deriving atomic charges: the RESP model. *J. Phys. Chem.* **1993**, *97*, 10269-10280.

14. Pearlman, D. A.; Case, D. A.; Caldwell, J. W.; Ross, W. S.; Cheatham, T. E.; DeBolt, S.; Ferguson, D.; Seibel, G.; Kollman, P. AMBER, a package of computer programs for applying molecular mechanics, normal mode analysis, molecular dynamics and free energy calculations to simulate the structural and energetic properties of molecules. *Comput. Phys. Commun.* **1995**, *91*, 1-41.

15. Case, D. A.; Cheatham, T. E.; Darden, T.; Gohlke, H.; Luo, R.; Merz, K. M.; Onufriev, A.; Simmerling, C.; Wang, B.; Woods, R. J. The Amber biomolecular simulation programs. *J. Comput. Chem.* **2005**, *26*, 1668-1688.

16. Gerlach, R. W.; Kowalski, B. R.; Wold, H. O. A. Partial least-squares path modelling with latent variables. *Anal. Chim. Acta.* **1979**, *112*, 417-421.

17. Cavalli, A.; Poluzzi, E.; De Ponti, F.; Recanatini, M. Toward a pharmacophore for drugs inducing the long QT syndrome: insights from a CoMFA study of HERG K(+) channel blockers. *J. Med. Chem.* **2002**, *45*, 3844-3853.

18. Zhou, Z.; Vorperian, V. R.; Gong, Q.; Zhang, S.; January, C. T. Block of HERG potassium channels by the antihistamine astemizole and its metabolites desmethylastemizole and norastemizole. *J. Cardiovasc. Electrophysiol.* **1999**, *10*, 836-843.

19. Wang, J.; Della Penna, K.; Wang, H.; Karczewski, J.; Connolly, T. M.; Koblan, K. S.; Bennett, P. B.; Salata, J. J. Functional and pharmacological properties of canine ERG potassium channels. *Am. J. Physiol. Heart Circ. Physiol.* **2003**, *284*, H256-267.

20. Ekins, S.; Crumb, W. J.; Sarazan, R. D.; Wikel, J. H.; Wrighton, S. A. Three-dimensional quantitative structure-activity relationship for inhibition of human ether-a-go-go-related gene potassium channel. *J. Pharmacol. Exp. Ther.* **2002**, *301*, 427-434.

21. Kiesecker, C.; Zitron, E.; Luck, S.; Bloehs, R.; Scholz, E. P.; Kathofer, S.; Thomas, D.; Kreye, V. A.; Katus, H. A.; Schoels, W.; Karle, C. A.; Kiehn, J. Class Ia anti-arrhythmic drug ajmaline blocks HERG potassium channels: mode of action. *Naunyn. Schmiedebergs. Arch. Pharmacol.* **2004**, *370*, 423-435.

22. Thomas, D.; Hammerling, B. C.; Wu, K.; Wimmer, A. B.; Ficker, E. K.; Kirsch, G. E.; Kochan, M. C.; Wible, B. A.; Scholz, E. P.; Zitron, E.; Kathofer, S.; Kreye, V. A.; Katus, H. A.; Schoels, W.; Karle, C. A.; Kiehn, J. Inhibition of cardiac HERG currents by the DNA topoisomerase II inhibitor amsacrine: mode of action. *Br. J. Pharmacol.* **2004**, *142*, 485-494.

23. Walker, B. D.; Singleton, C. B.; Tie, H.; Bursill, J. A.; Wyse, K. R.; Valenzuela, S. M.; Breit, S. N.; Campbell, T. J. Comparative effects of azimilide and ambasilide on the human ether-a-go-go-related gene (HERG) potassium channel. *Cardiovasc. Res.* **2000**, *48*, 44-58.

24. Witchel, H. J.; Pabbathi, V. K.; Hofmann, G.; Paul, A. A.; Hancox, J. C. Inhibitory actions of the selective serotonin re-uptake inhibitor citalopram on HERG and ventricular L-type calcium currents. *FEBS. Lett.* **2002**, *512*, 59-66.

25. Yuill, K. H.; Borg, J. J.; Ridley, J. M.; Milnes, J. T.; Witchel, H. J.; Paul, A. A.; Kozlowski, R. Z.; Hancox, J. C. Potent inhibition of human cardiac potassium (HERG) channels by the anti-estrogen agent clomiphene-without QT interval prolongation. *Biochem. Biophys. Res. Commun.* **2004**, *318*, 556-561.

26. Ferreira, S.; Crumb, W. J., Jr.; Carlton, C. G.; Clarkson, C. W. Effects of cocaine and its major metabolites on the HERG-encoded potassium channel. *J*. *Pharmacol*. *Exp*. *Ther*. **2001**, *299*, 220-226.

27. Davie, C.; Pierre-Valentin, J.; Pollard, C.; Standen, N.; Mitcheson, J.; Alexander, P.; Thong, B. Comparative pharmacology of guinea pig cardiac myocyte and cloned hERG (I(Kr)) channel. *J*. *Cardiovasc*. *Electrophysiol*. **2004**, *15*, 1302-1309.

28. Kuryshev, Y. A.; Brown, A. M.; Wang, L.; Benedict, C. R.; Rampe, D. Interactions of the 5-hydroxytryptamine 3 antagonist class of antiemetic drugs with human cardiac ion channels. *J*. *Pharmacol*. *Exp*. *Ther*. **2000**, *295*, 614-620.

29. Drolet, B.; Rousseau, G.; Daleau, P.; Cardinal, R.; Turgeon, J. Domperidone should not be considered a no-risk alternative to cisapride in the treatment of gastrointestinal motility disorders. *Circulation*. **2000**, *102*, 1883-1885.

30. Drolet, B.; Zhang, S.; Deschenes, D.; Rail, J.; Nadeau, S.; Zhou, Z.; January, C. T.; Turgeon, J. Droperidol lengthens cardiac repolarization due to block of the rapid component of the delayed rectifier potassium current. *J*. *Cardiovasc*. *Electrophysiol*. **1999**, *10*, 1597-1604.

31. Tie, H. Cellular mechanisms of QT prolongation and proarhythmia induced by non-antiarrhytmic drugs. University of New South Wales. **2002**.

32. Mbai, M.; Rajamani, S.; January, C. T. The anti-malarial drug halofantrine and its metabolite N-desbutylhalofantrine block HERG potassium channels. *Cardiovasc*. *Res*. **2002**, *55*, 799-805.

33. Traebert, M.; Dumotier, B.; Meister, L.; Hoffmann, P.; Dominguez-Estevez, M.; Suter, W. Inhibition of hERG K+ currents by antimalarial drugs in stably transfected HEK293 cells. *Eur*. *J*. *Pharmacol*. **2004**, *484*, 41-48.

34. Ridley, J. M.; Milnes, J. T.; Duncan, R. S.; McPate, M. J.; James, A. F.; Witchel, H. J.; Hancox, J. C. Inhibition of the HERG K+ channel by the antifungal drug ketoconazole depends on channel gating and involves the S6 residue F656. *FEBS. Lett*. **2006**, *580*, 1999-2005.

35. Gonzalez, T.; Arias, C.; Caballero, R.; Moreno, I.; Delpon, E.; Tamargo, J.; Valenzuela, C. Effects of levobupivacaine, ropivacaine and bupivacaine on HERG channels: stereoselective bupivacaine block. *Br. J. Pharmacol*. **2002**, *137*, 1269-1279.

36. Ridley, J. M.; Dooley, P. C.; Milnes, J. T.; Witchel, H. J.; Hancox, J. C. Lidoflazine is a high affinity blocker of the HERG K(+)channel. *J. Mol. Cell. Cardiol*. **2004**, *36*, 701-705.

37. Crumb, W. J., Jr. Loratadine blockade of K(+) channels in human heart: comparison with terfenadine under physiological conditions. *J. Pharmacol. Exp. Ther*. **2000**, *292*, 261-264.

38. Katchman, A. N.; Koerner, J.; Tosaka, T.; Woosley, R. L.; Ebert, S. N. Comparative evaluation of HERG currents and QT intervals following challenge with suspected torsadogenic and nontorsadogenic drugs. *J. Pharmacol. Exp. Ther*. **2006**, *316*, 1098-1106.

39. Kang, J.; Chen, X. L.; Wang, L.; Rampe, D. Interactions of the antimalarial drug mefloquine with the human cardiac potassium channels KvLQT1/minK and HERG. *J. Pharmacol. Exp. Ther*. **2001**, *299*, 290-296.

40. Su, Z.; Martin, R.; Cox, B. F.; Gintant, G. Mesoridazine: an open-channel blocker of human ether-a-go-go-related gene K+ channel. *J. Mol. Cell. Cardiol*. **2004**, *36*, 151-160.

41. Claassen, S.; Zunkler, B. J. Comparison of the effects of metoclopramide and domperidone on HERG channels. *Pharmacology*. **2005**, *74*, 31-36.

42. Kikuchi, K.; Nagatomo, T.; Abe, H.; Kawakami, K.; Duff, H. J.; Makielski, J. C.; January, C. T.; Nakashima, Y. Blockade of HERG cardiac K+ current by antifungal drug miconazole. *Br. J. Pharmacol*. **2005**, *144*, 840-848.

43. Taglialatela, M.; Pannaccione, A.; Castaldo, P.; Giorgio, G.; Annunziato, L. Inhibition of HERG1 K(+) channels by the novel second-generation antihistamine mizolastine. *Br. J. Pharmacol.* **2000**, *131*, 1081-1088.

44. Kim, K. S.; Kim, E. J. The phenothiazine drugs inhibit hERG potassium channels. *Drug. Chem. Toxicol.* **2005**, *28*, 303-313.

45. Wu, L. M.; Orikabe, M.; Hirano, Y.; Kawano, S.; Hiraoka, M. Effects of Na+ channel blocker, pilsicainide, on HERG current expressed in HEK-293 cells. *J. Cardiovasc. Pharmacol.* **2003**, *42*, 410-418.

46. Kongsamut, S.; Kang, J.; Chen, X. L.; Roehr, J.; Rampe, D. A comparison of the receptor binding and HERG channel affinities for a series of antipsychotic drugs. *Eur. J. Pharmacol.* **2002**, *450*, 37-41.

47. Siebrands, C. C.; Schmitt, N.; Friederich, P. Local anesthetic interaction with human ether-a-go-go-related gene (HERG) channels: role of aromatic amino acids Y652 and F656. *Anesthesiology*. **2005**, *103*, 102-112.

48. Tarantino, P.; Appleton, N.; Lansdell, K. Effect of trazodone on hERG channel current and QT-interval. *Eur. J. Pharmacol.* **2005**, *510*, 75-85.

49. Zitron, E.; Kiesecker, C.; Scholz, E.; Luck, S.; Bloehs, R.; Kathofer, S.; Thomas, D.; Kiehn, J.; Kreye, V. A.; Katus, H. A.; Schoels, W.; Karle, C. A. Inhibition of cardiac HERG potassium channels by the atypical antidepressant trazodone. *Naunyn. Schmiedebergs. Arch. Pharmacol.* **2004**, *370*, 146-156.

50. Cockerill, S. L.; Tobin, A. B.; Torrecilla, I.; Willars, G. B.; Standen, N. B.; Mitcheson, J. S. Modulation of hERG potassium currents in HEK-293 cells by protein kinase C. Evidence for direct phosphorylation of pore forming subunits. *J. Physiol.* **2007**, *581*, 479-493.